JACS
JOURNAL OF THE AMERICAN CHEMICAL SOCIETY
Article
pubs.acs.org/JACS

Conjugation-Driven "Reverse Mars–van Krevelen"-Type Radical Mechanism for Low-Temperature C–O Bond Activation

Alexander V. Mironenko and Dionisios G. Vlachos*

Department of Chemical and Biomolecular Engineering, Catalysis Center for Energy Innovation, University of Delaware, Newark, Delaware 19716, United States

Supporting Information

ABSTRACT: C–O bond activation on monofunctional catalysts (metals, carbides, and oxides) is challenging due to activity constraints imposed by energy scaling relationships. Yet, contrary to predictions, recently discovered multifunctional metal/metal oxide catalysts (e.g., Rh/ReO_x, Rh/MoO_x, Ir/VO_x) demonstrate unusually high C–O scission activity at moderate temperatures. Herein, we use extensive density functional theory calculations, first-principles microkinetic modeling, and electronic structure analysis to elucidate the metal/metal oxide synergy in the Ru/RuO_2 catalyst, which enables up to 76% yield of the C–O scission product (2-methyl furan) in catalytic transfer hydrogenolysis of furfural at low temperatures. Our key mechanistic finding is a facile radical-mediated C–O bond activation on RuO_2 oxygen vacancies, which directly leads to a weakly bound final product. This is the first time the radical *reduction* mechanism is reported in heterogeneous catalysis at temperatures <200 °C. We attribute the unique catalytic properties to the formation of a conjugation-stabilized furfuryl radical upon C–O bond scission, the strong hydroxyl affinity of oxygen vacancies due to the metallic character of RuO_2, and the acid–base heterogeneity of the oxide surface. The conjugation-driven radical-assisted C–O bond scission applies to any catalytic surface that preserves the π-electron system of the reactant and leads to C–O selectivity enhancement, with notable examples including Cu, H-covered Pd, self-assembled monolayers on Pd, and oxygen-covered Mo_2C. Furthermore, we reveal the cooperativity of active sites in multifunctional catalysts. The mechanism is fully consistent with kinetic studies and isotopic labeling experiments, and the insights gained might prove useful more broadly in overcoming activity constraints induced by energy scaling relationships.

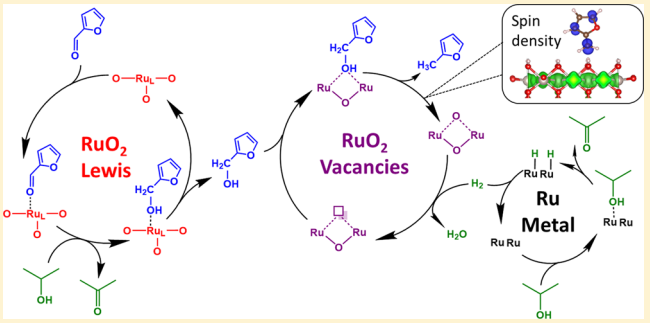

INTRODUCTION

Selective C–O bond scission is essential in various industrially important chemical processes. For example, in Fischer–Tropsch synthesis, which has experienced a revival due to the revolution of shale gas,[3] C–O bond activation can potentially govern the hydrocarbons-to-alcohols product ratio.[4,5] Selective C–O cleavage is also crucial in first-generation biofuels production, as it is implicated in the conversion of glycerol byproduct to the commodity chemical propylene glycol.[6] For emerging second-generation biofuels and chemicals, efficient oxygen removal is necessary for integration into the downstream oil refining infrastructure.[7]

Unlike reforming and dehydrogenation, which involve C–C and C–H bond breaking, the design of a selective C–O scission catalyst represents a significant challenge. Activity and selectivity maps for small oxygenates, such as ethylene glycol, indicate that the best deoxygenation metal catalysts would be orders of magnitude slower than good reforming catalysts under the same reaction conditions.[8,9] Experimental studies of ethanol conversion on group 8–11 transition metal catalysts of varying oxophilicity (Cu, Pt, Pd, Ir, Rh, Ru) confirm that reforming reactions are dominant and the yield to hydrocarbons (ethylene and ethane) is negligible.[10] Similarly, UHV experiments indicate that the rates of 1-propanol and ethylene glycol selective deoxygenation on oxophilic Mo(110)[11] and Mo_2C[12] surfaces are lower than that of C–C bond scission over reforming catalysts Ni(111) and Fe/Ni(111).[13] Late transition metals are deemed ineffective for C–O scission due to poisoning by the CO byproduct and requirement of large metal clusters.[14]

An alternative strategy for C–O bond activation utilizes reducible transition metal oxides. In the "reverse Mars–van Krevelen[15] mechanism", an oxide surface is being reduced by hydrogen to produce oxygen vacancies, which in turn abstract oxygen atoms from O-containing reactants, restoring the initial surface structure. Román-Leshkov and co-workers[16−18] found MoO_3 to be efficient for deoxygenation of ketones, furanics, and aromatics at low H_2 pressures with up to 98% selectivities. However, a temperature of 320 °C was required for the oxide to acquire sufficient deoxygenation activity. Similarly, oxygen vacancies of CeO_2–ZrO_2 were active for guaiacol conversion

Received: March 18, 2016
Published: June 9, 2016

DOI: 10.1021/jacs.6b02871
J. Am. Chem. Soc. 2016, 138, 8104–8113

above 325−350 °C,[19] and WO_3 bronzes were active for hydrodeoxygenation of acrolein above 300−350 °C.[20] There is a clear need for more active, low-temperature C−O bond activation catalysts.

Over the past few years, a plethora of transition metal/metal-oxide hybrid catalysts (TM/MO) has been developed, which, unlike metals and oxides alone, are capable of selectively and effectively catalyzing C−O bond scission at moderate temperatures (100−200 °C). Examples include glycerol hydrogenolysis to either 1,2-propanediol on Ru/ReO_x[21] and Rh/ReO_x[22] or 1,3-propanediol on Ir/ReO_x,[23] ring opening in tetrahydrofurfuryl alcohol on Ir/VO_x,[24] ring opening in tetrahydropyran-2-methanol on Rh-ReO_x to form 1,6-hexanediol,[25] and deoxygenation and ring-opening reactions in diols, triols, furans, and pyrans on Rh-ReO_x and Rh-MoO_x.[26]

The high C−O scission activity over many TM/MO catalysts for chemically and structurally different reactants hints to a potentially general C−O bond activation mechanism that remains poorly understood and occasionally controversial. Chia et al. proposed a Brønsted acid-catalyzed mechanism via oxocarbenium ions involving OH groups on Re single atoms incorporated into the Rh surface, based on NH_3 temperature-programmed desorption experiments and DFT calculations.[26] The proposed C−O bond scission with simultaneous hydride transfer from α-C to β-C as the rate-limiting step is at variance with a first-order reaction with respect to hydrogen and the observed deuterium incorporation at the β-C position in isotopic labeling experiments, carried out by Tomishige and co-workers for tetrahydrofurfuryl alcohol ring-opening.[27] Instead, a direct hydride attack mechanism occurring on the Rh (or Ir)/ReO_x interface was proposed. In the hydrodeoxygenation of furfuryl alcohol on Ru/RuO_2, isotopic labeling experiments[28] indicated oxygen removal with simultaneous furan ring activation by hydrogen. DFT calculations[1] clearly showed that RuO_2 Lewis acid sites are inefficient for C−O bond hydrogenolysis, but the active site and the role of Ru remained elusive.

In order to elucidate the TM/MO oxide synergy for C−O bond activation, here we investigate a model reaction system, namely the catalytic transfer hydrogenolysis (CTH) of furfural (FAL) to yield 2-methylfuran (2-MF) on the Ru/RuO_2 catalyst, using 2-propanol as a solvent and hydrogen donor (Scheme 1).

Scheme 1. Catalytic Transfer Hydrogenolysis (CTH) of Furfural (FAL) To Form 2-Methyl Furan (2-MF) Using 2-Propanol as a Hydrogen Donor[a]

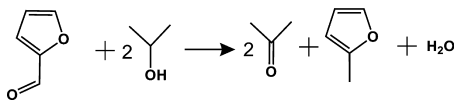

[a]The latter is converted to acetone.

2-MF yields of 76% at moderate temperatures (<200 °C) in the liquid phase,[29,30] unattainable on Ru and RuO_2 catalysts alone, were reported. 2-MF can be a renewable drop-in fuel or converted to jet fuels, lubricants,[31] and aromatics;[32,33] furfural is produced industrially from lignocellulosic biomass. We find a rather unexpected radical reverse Mars−van Krevelen-type mechanism over metal oxide vacancies that rationalize the high C−O bond hydrogenolysis activity. We show that a radical intermediate is a prerequisite for the facile C−O scission reaction, and this finding is consistent with the deuterium distribution in H/D labeling experiments and reactivities of aromatic vs aliphatic oxygenates. To the best of our knowledge, this is the first evidence for a radical *reduction* mechanism (as opposed to radical oxidation) in heterogeneous catalysis being operative at temperatures below 200−250 °C. We elucidate a rather complex, trifunctional behavior of a TM/MO catalyst: Lewis acid sites of RuO_2 convert furfural to furfuryl alcohol via the Meerwein−Ponndorf−Verley (MPV) mechanism; oxygen vacancies catalyze C−O bond hydrogenolysis; and metallic sites provide hydrogen for vacancy formation. High reaction rates, e.g., in C−O scission, can be linked to moderate oxophilicity of metallic or oxide surfaces via universal linear scaling relationships.[34−37] While RuO_2 vacancies exhibit lower O binding energy than metallic Ru(0001) sites, we find that the former are much more catalytically active in C−O scission and water formation. We attribute this counterintuitive catalyst behavior to a conjugation-stabilized radical intermediate, unusually strong hydroxyl affinity of oxygen vacancies due to the metallic character of RuO_2, and acid−base heterogeneity of the RuO_2 surface.

RESULTS AND DISCUSSION

C−O bond hydrogenolysis on Ru(0001) and RuO_2(110). We first explore furfural hydrogenation to furfuryl alcohol on Ru and RuO_2; both materials are effective in catalyzing the reaction, albeit via a different mechanism (see Figure S1). The metal follows a Horiuti−Polanyi-type sequential endothermic addition of coadsorbed hydrogen atoms to the C═O bond starting with C−H and followed by O−H bond formation, with the highest barrier of 1.0 eV in the latter step (Table S1, Figure S2). The oxide carries out direct intermolecular hydride transfer from 2-propanol to furfural via the MPV mechanism on Lewis acid sites.[1] The barrier in the MPV mechanism is only 0.2 eV, indicating that the RuO_2 is more efficient than Ru in C═O hydrogenation, consistent with isotopic tracing experiments and a kinetic isotope effect.[28]

Next, we turn to the hydrogenolysis reaction. Reaction pathway energetics for subsequent transformation of furfuryl alcohol to 2-MF on Ru(0001) and RuO_2(110)[1] surfaces are shown in Figure 1 (see Figure S2 and Table S1 for structures and energetics). On both surfaces, strongly adsorbed FCH_2OH (binding energies −2.5 and −1.8 eV, respectively) undergoes a facile O−H bond scission yielding a furoxy species, FCH_2O. The following C−O bond breaking on Ru(0001) is facile with a 0.7 eV barrier, and the resulting furfuryl species FCH_2 easily reacts with a hydrogen atom to form 2-MF that desorbs from the surface. The hydrogenolysis efficiency of the Ru(0001) surface is overshadowed by the difficulty of hydrogenating the produced surface oxygen atoms and completing the catalytic cycle, as the barriers for adding the first and second hydrogen atom to form water are 1.6 and 1.3 eV, respectively. The difficulty of removing oxygen from Ru surfaces below the 0.25 ML coverage is well-known in surface science studies[38,39] and lies in the high oxophilicity of metallic Ru. Our microkinetic modeling indicates that the oxygen coverage is > 0.25 ML (not shown); DFT calculations indicate that 0.25 ML O/Ru(0001) with a p(2 × 2) periodicity increases the C−O scission barrier in furoxy species by at least 0.8 eV compared to bare Ru (Table S1). On more open Ru nanoparticle facets and edges, the inhibition by surface oxygen is likely to be even more prominent due to lower metal coordination numbers.[40,41] In summary, the high oxophilicity of Ru, which leads to facile C−

DOI: 10.1021/jacs.6b02871
J. Am. Chem. Soc. 2016, 138, 8104−8113

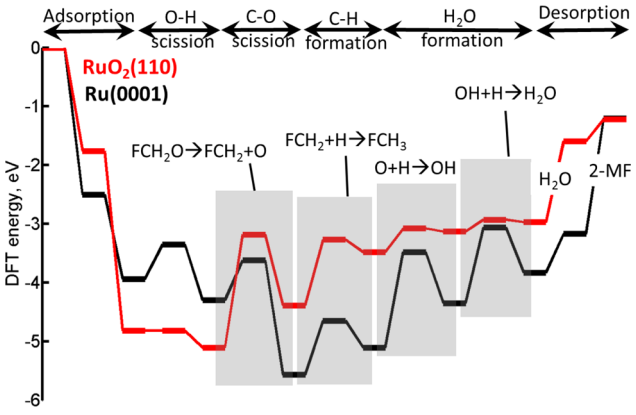

Figure 1. Minimum energy DFT reaction pathways for furfuryl alcohol conversion to 2-methyl furan (2-MF) on Ru(0001) (black) and RuO_2(110) (red) surfaces. All energies are referenced to furfuryl alcohol and H_2 in vacuum and bare Ru(0001) and RuO_2(110) slabs. F denotes the furan ring with H at the C_1 position removed (C_4H_3); O, H, OH, and H_2O refer to the corresponding chemisorbed species. Data for RuO_2 are taken from ref 1.

O bond scission, is also responsible for the slow formation of water and an increase in the deoxygenation barriers at higher oxygen coverages, leading to modest catalyst activity.

On RuO_2(110), on the other hand, the C−O scission barrier in FCH_2O over Ru_{cus} Lewis acid sites (see Scheme 2) is

Scheme 2. Top Two O−Ru−O Layers of a RuO_2(110) Surface[a]

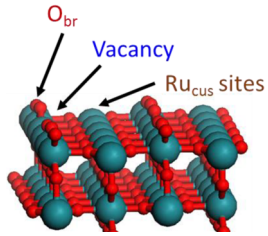

[a]Bridging oxygen (O_{br}), coordinatively unsaturated Ru sites (Ru_{cus}), and oxygen vacancies are shown.

prohibitively high (1.9 eV),[1] rendering the RuO_2 phase inefficient for activating C−O bonds. In addition, the RuO_2 surface binds water molecules strongly (1.4 eV desorption barrier). The above findings clearly show that neither Ru nor RuO_2 are active catalysts for hydrogenolysis in agreement with experiments,[29,42] and raise the question of which is the active site and the mechanism in these systems.

C−O bond hydrogenolysis active site. XANES/EXAFS results reveal that RuO_2 is being reduced to metallic Ru over the course of catalytic transfer hydrogenolysis.[42] Scanning tunneling microscopy (STM) experiments have shown[43,44] that RuO_2 reduction commences with formation of metallic Ru nanoclusters and patches on the oxide surface. Patches of one metal on the other are known to greatly enhance catalyst activity by coupling two different catalyst functionalities via surface spillover, e.g., in ammonia decomposition.[45] In the Ru/RuO_2 system, Ru is active in C−O bond breaking, and RuO_2 is effective in oxygen removal; however, due to large difference in oxygen binding energies (−0.5 vs + 0.8 eV on Ru(0001) and RuO_2 (110), respectively; Table S2), oxygen spillover is unlikely. Metal−metal oxide synergy has also been attributed to interfacial sites, for example, in CO oxidation on Au/TiO_2.[46] Our detailed calculations rule out this possibility as well. We found that the Ru/RuO_2 interface does not considerably enhance the Lewis acid oxophilicity; also, metallic Ru becomes even more oxophilic, exacerbating oxygen poisoning (Section S2). Consequently, the direct contact between Ru and RuO_2 phases is not advantageous for efficient C−O bond hydrogenolysis. A Brønsted acid-catalyzed mechanism is also thermodynamically unfavorable (Table S6, reaction 16). Our findings refute the most common synergy mechanisms on metal/metal oxide catalysts.

Oxygen vacancies play a vital role in a plethora of metal oxide-catalyzed chemical processes, such as methane oxidation on PdO_x/ZrO_2,[47] CO oxidation on Au- and ZrO_2- promoted CeO_2,[48,49] RuO_2,[50] and Pt_1/FeO_x,[51] or propene oxidation on bismuth molybdates.[52] RuO_2(110) forms vacancies already at room temperature upon H_2 exposure.[53] This motivated us to consider oxygen vacancies as a possible active site for low-temperature C−O bond hydrogenolysis.

The minimum energy pathway for furfuryl alcohol conversion to 2-MF over an oxygen vacancy is shown in Figure 2 (states A−D). Due to the extremely high affinity of

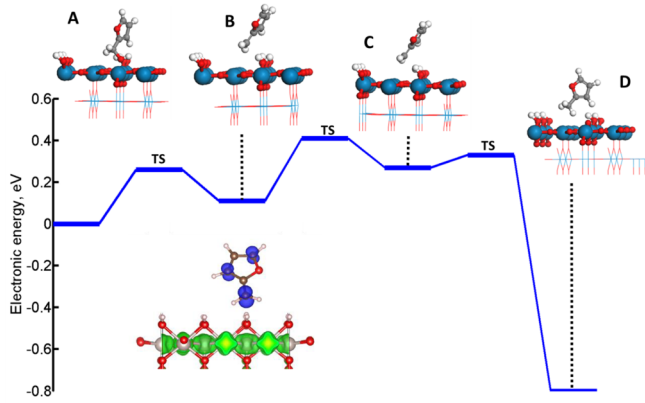

Figure 2. Minimum energy reaction pathway for C−OH bond scission in furfuryl alcohol, adsorbed over a vacancy on a hydroxylated RuO_2(110) surface, along with associated structures. One possibility for H abstraction by a furfuryl radical is shown; due to its weak interaction with the surface, furfuryl can migrate along the surface and react with more remote hydroxyls. The inset depicts unpaired electron density (spin 1/2 minus spin −1/2) for state B. Blue denotes areas with dominant localization of S = −1/2 electrons; green, with S = 1/2 electrons. Bader sphere-projected atomic spin densities on C1, C3, and C5 atoms are 0.41, 0.23, and 0.21 Bohr-magnetons, respectively.

O_{br} surface sites toward hydrogen (−3.8 eV H binding energy vs −2.7 to −3 eV on group 8−10 transition metals[54]), all O_{br} are capped by hydrogen atoms via a low-barrier (<0.5 eV), highly exothermic hydrogen abstraction from the 2-propanol solvent (Table S6). Furfuryl alcohol chemisorption occurs via the OH group to the vacancy in a mildly exothermic step (binding energy −0.8 eV). The positive total Bader charge of the alcohol molecule (+0.09) reveals minor electron donation to the surface, indicating that the vacancy acts as a Lewis acid, similar to neighboring Ru_{cus} sites (see Table S7). The subsequent C−OH scission is highly favorable, with a reaction barrier of 0.3 eV. The leaving OH group annihilates the oxygen vacancy, leaving behind a weakly adsorbed furfuryl fragment FCH_2 (−0.3 eV binding energy). Followed by OH group rotation with a barrier of ∼0.3 eV (state B−C), the furfuryl

DOI: 10.1021/jacs.6b02871
J. Am. Chem. Soc. 2016, 138, 8104−8113

fragment reacts with surface hydroxyl (0.1 eV barrier), resulting in a physisorbed final product −2-MF (−0.4 eV binding energy). The reaction can proceed in a single concerted step or may involve migration of the weakly bound furfuryl fragment to neighboring hydroxyls. Favorable reaction energetics makes it clear that oxygen vacancies are by far the most active sites in deoxygenation.

Even more interestingly, the spin electron density plotted for state B (inset of Figure 2) displays localization of an unpaired electron on a furfuryl fragment at the C_1, C_3, and C_5 positions, indicating the formation of a furfuryl radical intermediate over the course of the reaction. Radical intermediates on oxide surfaces are ubiquitous in catalytic oxidation of alkanes and alkenes,[55−59] yet this chemistry frequently involves C−H scission barriers >1 eV and thus requires high temperatures (>300 °C) in order to achieve appreciable reaction rates. The low barrier in the C−OH scission signifies that radicals can also mediate heterogeneous catalytic processes involving reduction, potentially at much lower temperatures (<200 °C). However, the feasibility of the radical reduction mechanism depends on the catalyst effectiveness and its ability to complete the catalytic cycle. This is discussed next.

Vacancy formation mechanism on RuO_2(110). The vacancy-mediated C−O bond hydrogenolysis demands continuous *in situ* regeneration of the catalytic sites, and a key step in this cycle is vacancy formation. Vacancy formation has been suggested to occur via the removal of the bridging $O_{br}H$ group by a neighboring H atom adsorbed on a Ru_{cus} site, forming a H_2O molecule on Ru_{cus}.[53] Our DFT calculations could not identify a transition state with a <2 eV reaction barrier; the difficulty of removing $O_{br}H$ is likely due to its strong binding to the surface (−4.0 eV binding energy over a vacancy). Vacancy formation from two neighboring $O_{br}H$ groups, suggested for TiO_2 (110),[60] is also unfavorable (Table S6, reaction 4). It is clear that the typically postulated mechanisms for vacancy formation are ineffective.

In order to elucidate the mechanism, consistent with vacancy formation at room temperature, we investigated computationally several possible ways a hydrogen molecule can react with a nonhydroxylated[1] and a hydroxylated RuO_2(110) surface (Table S6), leading to vacancy formation. The microkinetic model (Section S3), containing all such reactions, reproduces well all essential features observed upon 100 Langmuir H_2 exposure at 25 °C using STM/X-ray photoelectron spectroscopy (XPS). In particular, we find OH_{br} hydroxyls to be dominant on the surface; transformation of ∼5% O_{br} to vacancies; and formation of water molecules on Ru_{cus} sites (Table S8). The model also reproduces an experimental two-peak temperature-programmed desorption/reduction H_2O profile quite well (Figure S5). Reaction path analysis reveals a rather novel, low-temperature vacancy formation mechanism that begins with associative adsorption of H_2 on Ru_{cus} of a hydroxylated surface (−0.5 eV binding energy), followed by a slightly endothermic (ΔE = +0.2 eV), low-barrier (0.4 eV), heterolytic H_2 splitting to form coadsorbed H on Ru_{cus} and H_2O_{br} water-like species (Figure 3). H can subsequently react with OH_{br} to form H_2O_{br}. Unlike O_{br} and $O_{br}H$, H_2O_{br} is weakly bound to the surface (−0.6 eV binding energy), and thus can either desorb as water or migrate to a proximal vacant Ru_{cus} site (0.4 eV barrier, −0.6 eV exothermic), resulting in vacancy formation in both scenarios. The microkinetic model indicates that the surface coverage of H_2O_{br} never exceeds 10^{-11} ML (a reactive precursor) and rationalizes the lack of observing it in STM and XPS studies, which led to the postulate that this is not an important precursor.[53,61] Taken together, DFT and microkinetic simulation provide strong evidence for a vacancy formation mechanism with the H_2O_{br} species as a vacancy precursor.

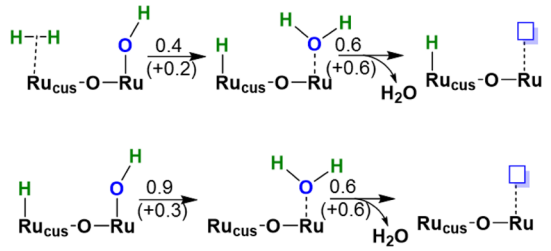

Figure 3. Vacancy formation mechanism, as determined by the reaction path analysis in the microkinetic model. Reaction barriers (reaction energies) in eV.

Multifunctional catalytic mechanism. One important question is how the hydrogen donor forms the H_2O_{br} species. We believe that there are two important contributions. First, 2-propanol can easily form a fully hydroxylated surface, with all O_{br} capped with H. Upon hydroxylation, the OH_{br} is no longer able to dehydrogenate alcohol: final states for sequential C−H/O−H scission cannot be identified using DFT, whereas the simultaneous C−H/O−H bond scission is 1.2 eV endothermic. Second, small amounts of hydrogen, produced *in situ* during CTH hydrogenolysis on metallic Ru from dehydrogenation of 2-propanol[2,62] (due to the ineffectiveness of the hydroxylated RuO_2), generate vacancies as discussed above, which catalyze the hydrogenolysis of furfuryl alcohol, completing the catalytic cycle (Figure 4a). While the metallic Ru surface can partially be oxidized due to high reaction barriers for removal of surface oxygen (Figure 1), at the 0.25 ML O/Ru(0001) coverage, the C−O bond scission is inhibited (Table S1, reactions 10−11), preventing further surface oxidation and making metallic Ru sites available for H_2 production. In contrast, C−H and O−H bond scission reactions, involved, for example, in 2-propanol dehydrogenation, can still proceed on the 0.25 ML O/Ru(0001) surface.[63]

Starting with furfural as a reactant, Ru/RuO_2 exposes trifunctional catalysis: furfural is converted to furfuryl alcohol on Ru_{cus} Lewis acidic sites of RuO_2 via the MPV mechanism;[28] furfuryl alcohol undergoes C−OH scission on RuO_2 oxygen vacancies, forming 2-MF and oxidizing the vacancy; and finally, H_2 is produced on metallic Ru sites via dehydrogenation of the hydrogen donor. H_2 in turn regenerates vacancies and closes the catalytic cycle (Figure 4b). The highest reaction barrier on each of three catalytic sites is lower than 0.9 eV, rendering the reaction mechanism feasible at moderate reaction temperatures <200 °C. An advantage of having a hydrogen donor, instead of external hydrogen, is that it enables selective carbonyl group hydrogenation via the MPV scheme, and the small amount of H_2, generated over the course of the reaction, prevents rapid reduction of the oxide catalyst, which will render the catalyst ineffective.

The microkinetic model for furfuryl alcohol hydrogenolysis (Section S4) reproduces well an experimental second order rate constant (0.016 L mol^{-1} h^{-1}),[28] if the ratio between the Ru and RuO_2 catalytic surface areas is ∼3 × 10^{-4}, consistent with the fresh catalyst predominantly composed of RuO_2. Sensitivity analysis (Table S9) reveals the overall hydrogenolysis rate to be governed by hydrogen generation from 2-propanol on metallic

DOI: 10.1021/jacs.6b02871
J. Am. Chem. Soc. 2016, 138, 8104−8113

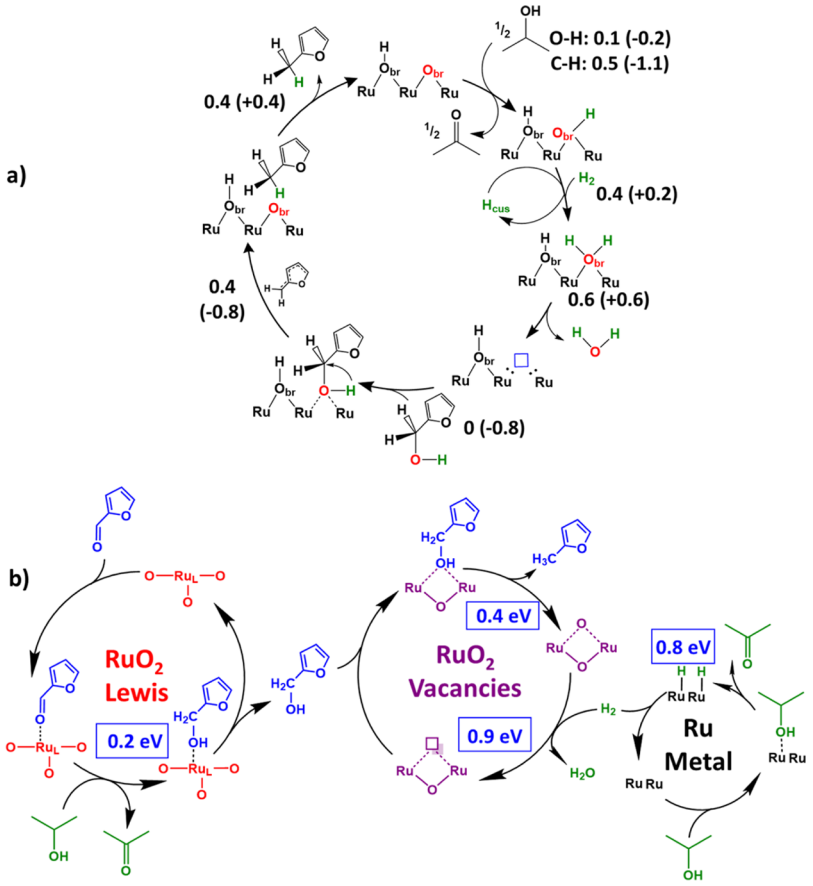

Figure 4. (a) Mars–van Krevelen-type reaction mechanism of furfuryl alcohol hydrogenolysis over the oxygen vacancies of the RuO_2(110) surface. DFT-based reaction barriers (energies) in eV. Associative adsorption steps are assumed to be nonactivated. Desorption barriers are taken as equal to the absolute values of the species binding energies. Two variants of the vacancy formation mechanism (involving H_{cus} or H_{2cus} ; Figure 3) and H abstraction from 2-propanol/propoxy by O_{br} are shown in an abbreviated form. (b) Synergy of Ru and RuO_2 active sites for hydrogenolysis of furfural. Numbers indicate the highest reaction barrier (in eV) for each cycle. The barrier over Ru_{cus} (Lewis acid sites) are taken from ref 1, and the dehydrogenation barrier over metallic Ru is taken from ref 2.

Ru sites. 2-Propanol dehydrogenation as a rate-limiting step conforms to an experimentally observed effect of hydrogen donor dehydrogenation activity on the hydrogenolysis rate[30] and is consistent with the kinetic isotope effect upon replacement of the hydrogen donor with its fully deuterated counterpart.[28]

Deuterated 2-propanol leads to incorporation of deuterium in both the C_1 (methyl group) and C_3 (furanic ring) positions of 2-MF.[28] However, the reasons for such incorporation have remained elusive. The inset of Figure 2 shows that the furfuryl radical intermediate possesses an unpaired electron delocalized between C_1, C_3, and C_5. Consequently, both C_1 and C_3 are susceptible to the D attack, whereas the C_5 atom is likely distant from the surface, particularly in a crowded surface environment of a liquid phase reaction. D addition to C_3 has a negligible barrier (0.07 eV) and is isoenergetic (+0.01 eV; Figure 5). We included the corresponding D addition/H removal steps into a microkinetic model (Section S4) and simulated mass-spectrometric peaks, with results shown in Figure 6. The first-principles model quantitatively predicts D incorporation into the ring of ∼40% of 2-MF molecules. m/z = 82 and m/z = 85 amu peaks demonstrate excellent agreement with the experiment. Underestimation of the m/z = 83 amu peak is likely caused by the not-accounted reaction FCHDOD + 2H → FCH_2D + DHO due to the presence of a mobile protium source in the system, e.g., OH_{br} groups on a fresh

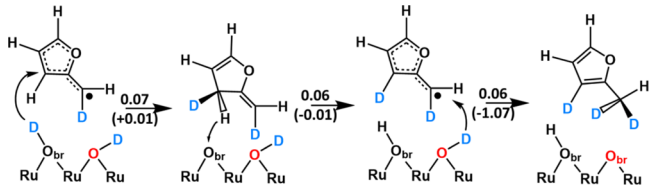

Figure 5. Mechanism of deuterium incorporation at the C_1 and C_3 positions of 2-MF. Numbers in parentheses indicate DFT reaction barriers (energies) in eV.

RuO_2 catalyst surface. When FCH_2OH containing mobile hydroxyl protium is used as a feed, the m/z = 82 amu peak due to the corresponding reaction $FCH_2OH + 2H \rightarrow FCH_3 + H_2O$ dominates, consistent with this explanation. Agreement between simulated and experimental mass-spectrometric peaks provides strong evidence for the radical C–O bond scission mechanism over RuO_2 vacancies.

Factors governing the reverse Mars van Krevelen mechanism on RuO_2(110) vacancies. Due to the high reducibility of RuO_2 and weak Ru–O_{br} bonds (Table S2), the ability of RuO_2 vacancies to break the C–O bond and be oxidized by furfuryl alcohol is at first counterintuitive. The bond-breaking activity of a catalyst is usually attributed to the binding strength of the final products to the surface;[35] yet in the C–O hydrogenolysis, one of the products, furfuryl radical,

DOI: 10.1021/jacs.6b02871
J. Am. Chem. Soc. 2016, 138, 8104–8113

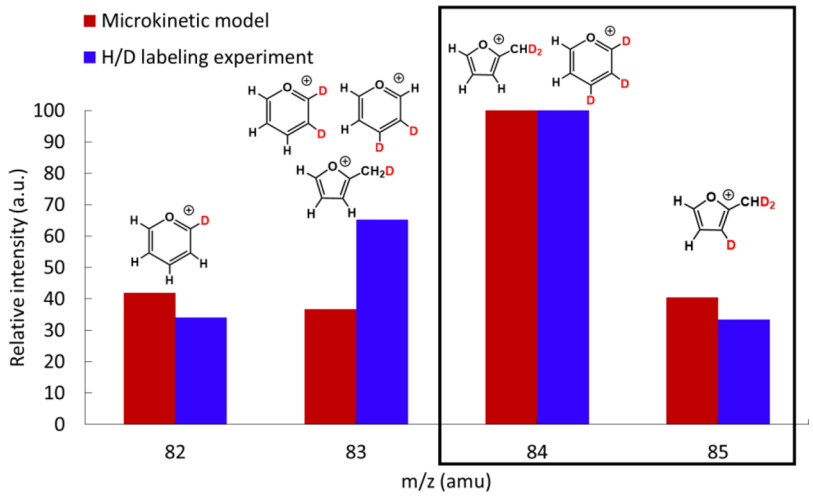

Figure 6. Comparison of experimental and simulated mass fragmentation spectra for furfuryl alcohol hydrogenolysis using fully deuterated 2-propanol as a hydrogen donor. Dominant contributions from fragments are shown. FCHDOD, formed by the MPV hydride transfer, is considered a reactant, where F is a furyl fragment C_4H_3O.

interacts weakly with the surface. A higher OH binding energy on a RuO_2 vacancy than on Ru(0001) surface (−0.8 vs −0.4 eV with respect to H_2O and 1/2 H_2) implies OH removal should be more difficult on RuO_2. In contrast to our expectation, O/OH removal from metallic Ru is hard, and vacancy formation on RuO_2 is very facile. We performed a detailed analysis of C−O bond hydrogenolysis energetics and identified three factors responsible for the unusual reactivity of RuO_2.

First, the intact π-electron (aromatic) system in the β-position to the C_1−O bond in adsorbed furfuryl alcohol is essential for high hydrogenolysis rates. Fully saturated compounds, e.g., 2-propanol and tetrahydrofurfuryl alcohol, exhibit much higher C−O scission barriers (1.4 eV) and give limited activity in experiments.[64] To gain further insight into the role of aromaticity, in Table 1 and Figure 7 we report the

Table 1. Born−Haber Decomposition of Adsorption/C−O Scission of Furfuryl Alcohol and Tetrahydrofurfuryl Alcohol over an Oxygen Vacancy[a]

Reactant	Furfuryl alcohol	Tetrahydrofurfuryl alcohol
$E_{ads\text{-}reactant}$	−0.8	−1.1
$E_{IS\text{-}FS}$	0.1	1.4
E_{C-O}	4.8	4.7
E_{relax}	−1.2	−0.3
E_{Ru-OH}	−4.0	−4.0
$E_{ads\text{-}radical}$	−0.3	−0.1

[a]Energies in eV.

results of the Born−Haber energy decomposition analysis for C−O bond hydrogenolysis in the aromatic (furfuryl alcohol) and the corresponding aliphatic (tetrahydrofurfuryl alcohol) compounds. Starting with reactants in a vacuum and a hydroxylated RuO_2(110) slab with a vacancy as an initial state, we separated the adsorption ($E_{ads\text{-}reactant}$)/C−O scission ($E_{IS\text{-}FS}$) reaction sequence into the following contributions (Figure 7b): (1) C−O scission in a vacuum with the frozen geometry of a furanic fragment (E_{C-O}); (2) relaxation of the furanic radical in a vacuum (E_{relax}); (3) adsorption of OH on a vacancy (E_{Ru-OH}); and (4) adsorption of the furanic radical over OH ($E_{ads\text{-}radical}$). Both furanic alcohols exhibit similar C−O bond scission energies in a vacuum (E_{C-O} = 4.7−4.8 eV), due to cleavage of an ordinary bond. The two species primarily differ in the relaxation energies E_{relax} of their radicals in a vacuum: −0.3 vs −1.2 eV for saturated and unsaturated radicals, respectively. Relaxation of the radical entails sp^3-to-sp^2 rehybridization of the C_1 atom; if the C_2 atom (β-carbon) is also sp^2-hybridized, a favorable ppπ overlap occurs (conjugation) between the C_1-localized p-orbital and the π-system of the furanic ring, as illustrated using crystal orbital Hamilton population analysis (COHP)[65−67] in Figure 8. Conjugation leads to delocalization of an unpaired electron (Figure 2) and stabilizes the furfuryl radical, effectively lowering the C−O scission barrier.

Unlike metals, where the furan ring strongly adsorbs on and partially loses its sp^2 character, the ring does not form strong covalent bonds with the RuO_2 surface and retains its gas-like geometry (Figure S4). Consequently, no side reactions (ring hydrogenation, decarbonylation, and ring opening) occur;[29] the furan aromatic ring remains intact under reaction conditions and facilitates C−O scission. Enhanced C−O scission rates have been related to the lack of π-system interaction with a metallic surface for furfuryl, benzyl,[68] and allyl alcohols[69] on a variety of catalytic systems, including Cu,[70−72] self-assembled monolayers on Pd,[73] H-covered Pd,[74] and partially oxidized Mo_2C.[75,76] Considering this literature data and our data together, the conjugation-assisted radical mechanism for activation of the C−O bond is a general one, provided that the π-electron system is preserved upon interaction of a molecule with a surface.

The second crucial factor of the high RuO_2 activity is the anomalously high stability of the OH group on a vacancy. Ru(0001) surface and RuO_2(110) vacancies differ in O binding energies (−0.5 vs +0.8 eV; Table S2). The universality of a linear scaling relationship between species binding energies for metals and oxides with octahedral coordination of ligands[36,37] implies that a RuO_2 vacancy should exhibit a OH binding energy of ∼0.2 eV (0 eV for a hydroxylated surface). Contrary to expectation, the OH binding energy is −1.1 eV (−0.8 eV on a hydroxylated RuO_2 surface). As a consequence, this strong binding significantly stabilizes the C−O scission intermediate (Table 1).

DOI: 10.1021/jacs.6b02871
J. Am. Chem. Soc. 2016, 138, 8104−8113

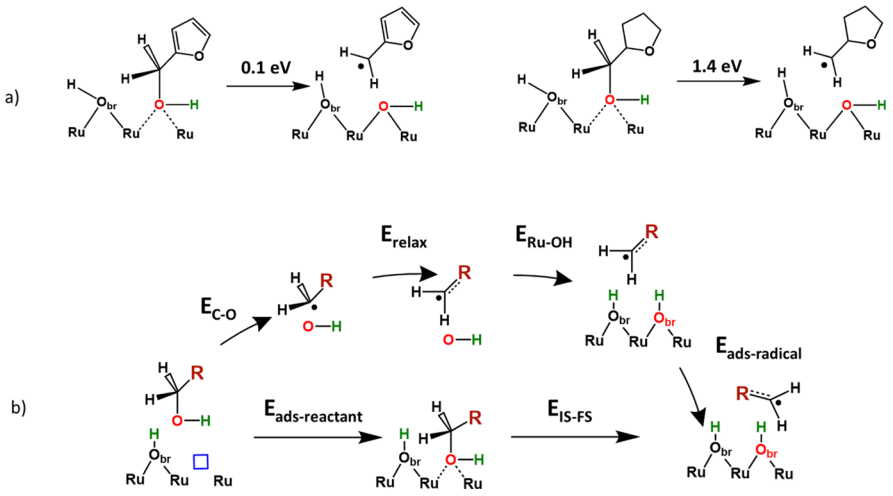

Figure 7. (a) C−O bond scission in furfuryl or tetrahydrofurfuryl alcohols; (b) Born−Haber cycle for the C−O scission mechanism over an oxygen vacancy. R denotes either a furfuryl or a tetrahydrofurfuryl fragment.

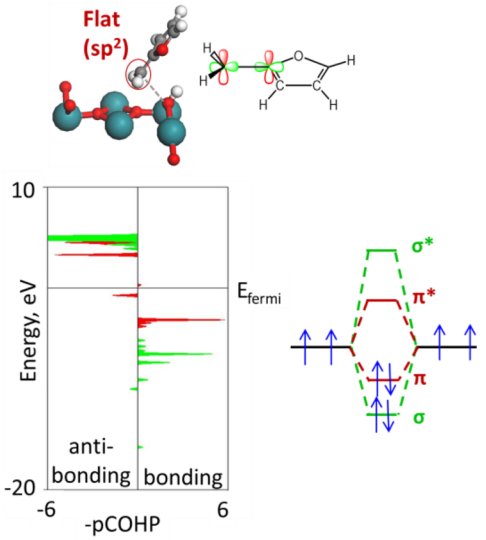

Figure 8. Crystal orbital Hamilton population (COHP) of the C_1−C_2 bond in furfuryl radical near the RuO_2(110) surface. ppσ overlap is denoted by green, ppπ overlap by red.

The origin of the extraordinary stability of the surface hydroxyl is revealed by considering the OH formation from O_{br} and H as a two-step process:[77,78] (1) excitation of an electron from an O-localized valence band to a metal-localized conduction band, forming an O^- surface radical; and (2) facile H abstraction by a radical. The energetics of step 1 has been shown to correlate with the electronic band gap for bismuth molybdates;[77,78] in addition, O-centered radicals were found to be crucial as abstracting sites for H transfer reactions.[79] Due to the lack of the band gap in RuO_2, surface O_{br}^- radicals are stable already at the ground electronic state (Figure S7), leading to high OH stability relative to O_{br} on RuO_2 vacancies and consequently to high C−O scission rates.

Given that OH is so stable on RuO_2, a natural question is why H + OH → H_2O reduction on the metal involves a 1.3 eV energy barrier, whereas on RuO_2 the H_{2cus} + $O_{br}H$ → H_{cus} + H_2O_{br} barrier is only 0.4 eV. First of all, water formation on the metal involves cleavage of strong M−H bonds (H binding energy of −3 eV on Ru(0001)), whereas on the oxide, H transfer to the neighboring hydroxyl occurs from adsorbed H_2 on Ru_{cus}, in which antibonding orbitals are partially populated and the H−H bond is weakened[80] (the energy of removing H from $H_{2,cus}$ and leaving H_{cus} on the surface is 2.6 eV). However, the major difference in water formation barriers stems from a transition state (de)stabilization mechanism. On the metallic Ru, the high H + OH → H_2O barrier is associated with overcoming Pauli repulsion during the O−H bond formation, which *destabilizes* the transition state.[81] On RuO_2, two opposite ends of the H_2 molecule in the transition state interact with Lewis-acidic Ru_{cus} and Lewis-basic $O_{br}H$ sites, forming a dipole (Bader charges −0.29 and +0.40, respectively). Consequently, favorable acid−base interaction reduces Pauli repulsion, and the transition state is *stabilized* by strong interaction with the surface (−2.1 eV with respect to H_2 in a vacuum in its transition state geometry), which largely compensates the energy penalty arising from H−H bond stretching (0.9 eV) and slab deformation (1.1 eV).[82] Therefore, the dual Lewis acid−base site nature of the RuO_2(110) surface leads to facile reduction and removal of surface hydroxyls, constituting the third reactivity factor. In fact, vacancy formation via OH removal is too facile on RuO_2, causing its rapid reduction under experimental conditions.[29,42] Therefore, optimization of oxide acid−base properties and hydroxyl stability will be essential for designing a more stable C−O hydrogenolysis catalyst.

CONCLUSIONS

We demonstrated that high 2-methyl furan yields achieved in catalytic transfer hydrogenation of furfural with 2-propanol stem from the interplay of three catalytic functionalities: RuO_2 Lewis acid sites that catalyze intermolecular hydride transfer, RuO_2 oxygen vacancies that promote C−O bond scission, and metallic Ru sites, which are essential for maintaining dissolved H_2 concentration and continuous vacancy regeneration. The most crucial step of the mechanism is ultrafast and selective reduction of the C−O bond over RuO_2 vacancies. We attribute the surprisingly high reduction activity of vacancies to a furfuryl radical intermediate. We employed an energy decomposition scheme and singled out three important factors governing catalyst activity toward C−O bond activation: favorable ppπ orbital overlap in the furfuryl radical intermediate, which retains its π-electron system near the catalyst surface and is thus stabilized by conjugation; high hydroxyl affinity of RuO_2

DOI: 10.1021/jacs.6b02871
J. Am. Chem. Soc. 2016, 138, 8104−8113

vacancies, attributed to the RuO_2 metallic character and the presence of O^-_{br} radical species in the ground state of the pristine surface; and acid−base heterogeneity of the surface, essential for H_2 dissociation and rapid vacancy formation. The radical mechanism is consistent with location-specific incorporation of deuterium into the furan ring in isotopic labeling experiments and explains the reactivity trends among aromatic/aliphatic compounds. The mechanism extends to other catalytic and reaction systems, provided that unsaturated reaction intermediates weakly interact with catalytic surfaces and retain their conjugated π-electron orbitals. The discovered conjugation-driven mechanism opens up opportunities for an integrated design of reaction pathways and catalytic materials, and can be beneficial for development of low-temperature catalytic processes, where small activation barriers are required.

METHODOLOGY

Density functional theory (DFT) calculations. Reaction energetics on Ru(0001) and RuO_2(110) model catalytic surfaces were calculated using the DFT Vienna ab initio simulation package (VASP) code, version 5.3.3.[83−86] The Ru(0001) surface was modeled as a four-layer p(4 × 4) slab with two bottom layers fixed in their bulk positions. The RuO_2(110) surface has been cleaved along the (110) crystal plane, which is known to possess the lowest surface energy[87] and has been observed experimentally.[42,50] We employed the p(3 × 2) supercell with four O−Ru−O stoichiometric trilayers along the z-direction. Three top atomic layers (O−Ru−O) were allowed to relax during optimization of ionic degrees of freedom, with the remaining atoms held fixed. Since ruthenium oxide (IV) belongs to a class of metallic oxides with substantial electron delocalization and no band gap,[88] reasonable performance of the GGA approximation can be expected. In this work, we use the exchange-correlation functional by Perdew, Burke, and Ernzerof (PBE)[89] for both Ru and RuO_2 surfaces, which has been shown to yield an accurate RuO_2 electronic structure[90] and RuO_2(110) reaction energetics in agreement with experimental data.[91] Grimme's dispersion correction, D3,[92] has been added to account for noncovalent interactions of the furan ring with the surface. Further computational details and benchmarking of vacancy formation energetics are reported in Section S1 of the SI.

First-principles-based microkinetic model. Microkinetic models for vacancy formation under ultrahigh vacuum conditions and furfuryl alcohol hydrogenolysis on RuO_2 in a liquid phase environment of a batch reactor were set up using an in-house Fortran code built around CHEMKIN.[93,94] Lists of elementary reactions, reaction conditions, calculations of reaction orders and the apparent activation energy, and all simulation details can be found in the SI.

ASSOCIATED CONTENT

Supporting Information

The Supporting Information is available free of charge on the ACS Publications website at DOI: 10.1021/jacs.6b02871.

Details of the DFT setup; benchmarking of vacancy formation energetics; reaction energies, barriers, and structures on Ru(0001) and RuO_2(110) surfaces; analysis of cooperativity effects of Ru and RuO_2(110) in contact with each other; total Bader charge of a furfuryl alcohol molecule on a vacancy; details of the microkinetic model of RuO_2(110) surface reduction at ultrahigh vacuum conditions and its comparison with experiments; specifications and assumptions of the microkinetic model of furfuryl alcohol catalytic transfer hydrogenolysis in a batch reactor, sensitivity analysis results, calculations of reaction orders with respect to 2-propanol and furfuryl alcohol, and the apparent activation energy; spin density localization on O_{br} sites of pristine RuO_2(110); (PDF)

Thermodynamic information for all liquid and surface species in a form of NASA polynomials (THERMDAT files); atomic coordinates of initial, transition, and final states in the CONTCAR file format and the corresponding total energies (XLSX, ZIP)

AUTHOR INFORMATION

Corresponding Author

*vlachos@udel.edu

Notes

The authors declare no competing financial interest.

ACKNOWLEDGMENTS

We acknowledge support from the Catalysis Center for Energy Innovation, an Energy Frontier Research Center funded by the U.S. Department of Energy, Office of Science, Office of Basic Energy Sciences under Award number DE-SC0001004. This research used resources of the National Energy Research Scientific Computing Center, a DOE Office of Science User Facility supported by the Office of Science of the U.S. Department of Energy under Contract No. DE-AC02-05CH11231. The authors acknowledge valuable discussions with Glen Jenness, Bingjun Xu, Konstantinos Goulas, and Matthew Gilkey. We also thank Zhaojia Lin, Abhay Athaley, and Marianthi Ierapetritou for assistance with ASPEN Plus.

REFERENCES

(1) Jenness, G. R.; Vlachos, D. G. *J. Phys. Chem. C* **2015**, *119*, 5938−5945.
(2) Mironenko, A. V.; Gilkey, M. J.; Panagiotopoulou, P.; Facas, G.; Vlachos, D. G.; Xu, B. *J. Phys. Chem. C* **2015**, *119*, 6075−6085.
(3) Gabriel, K. J.; Noureldin, M.; El-Halwagi, M. M.; Linke, P.; Jiménez-Gutiérrez, A.; Martínez, D. Y. *Curr. Opin. Chem. Eng.* **2014**, *5*, 49−54.
(4) Ishida, T.; Yanagihara, T.; Liu, X.; Ohashi, H.; Hamasaki, A.; Honma, T.; Oji, H.; Yokoyama, T.; Tokunaga, M. *Appl. Catal., A* **2013**, *458*, 145−154.
(5) Zhuo, M.; Borgna, A.; Saeys, M. *J. Catal.* **2013**, *297*, 217−226.
(6) Ma, F.; Hanna, M. A. *Bioresour. Technol.* **1999**, *70*, 1−15.
(7) Mortensen, P. M.; Grunwaldt, J.-D.; Jensen, P. A.; Knudsen, K.; Jensen, A. D. *Appl. Catal., A* **2011**, *407*, 1−19.
(8) Salciccioli, M.; Vlachos, D. G. *ACS Catal.* **2011**, *1*, 1246−1256.
(9) Vlachos, D. G. *AIChE J.* **2012**, *58*, 1314−1325.
(10) Ferrin, P.; Simonetti, D.; Kandoi, S.; Kunkes, E.; Dumesic, J. A.; Nørskov, J. K.; Mavrikakis, M. *J. Am. Chem. Soc.* **2009**, *131*, 5809−5815.
(11) Myint, M.; Chen, J. G. *ACS Catal.* **2015**, *5*, 256−263.
(12) Yu, W.; Salciccioli, M.; Xiong, K.; Barteau, M. A.; Vlachos, D. G.; Chen, J. G. *ACS Catal.* **2014**, *4*, 1409−1418.
(13) Myint, M.; Yan, Y.; Chen, J. G. *J. Phys. Chem. C* **2014**, *118*, 11340−11349.
(14) Gürbüz, E. I.; Hibbitts, D. D.; Iglesia, E. *J. Am. Chem. Soc.* **2015**, *137*, 11984−11995.
(15) Mars, P.; Van Krevelen, D. W. *Chem. Eng. Sci.* **1954**, *3*, 41−59.
(16) Prasomsri, T.; Nimmanwudipong, T.; Román-Leshkov, Y. *Energy Environ. Sci.* **2013**, *6*, 1732−1738.
(17) Prasomsri, T.; Shetty, M.; Murugappan, K.; Román-Leshkov, Y. *Energy Environ. Sci.* **2014**, *7*, 2660−2669.
(18) Shetty, M.; Murugappan, K.; Prasomsri, T.; Green, W. H.; Román-Leshkov, Y. *J. Catal.* **2015**, *331*, 86−97.
(19) Schimming, S. M.; LaMont, O. D.; König, M.; Rogers, A. K.; D'Amico, A. D.; Yung, M. M.; Sievers, C. *ChemSusChem* **2015**, *8*, 2073−2083.

DOI: 10.1021/jacs.6b02871
J. Am. Chem. Soc. 2016, 138, 8104−8113

(20) Thibodeau, T. J.; Canney, A. S.; DeSisto, W. J.; Wheeler, M. C.; Amar, F. G.; Frederick, B. G. *Appl. Catal., A* **2010**, *388*, 86−95.
(21) Ma, L.; He, D. *Catal. Today* **2010**, *149*, 148−156.
(22) Amada, Y.; Koso, S.; Nakagawa, Y.; Tomishige, K. *ChemSusChem* **2010**, *3*, 728−736.
(23) Nakagawa, Y.; Shinmi, Y.; Koso, S.; Tomishige, K. *J. Catal.* **2010**, *272*, 191−194.
(24) Pholjaroen, B.; Li, N.; Huang, Y.; Li, L.; Wang, A.; Zhang, T. *Catal. Today* **2015**, *245*, 93−99.
(25) Chen, K.; Koso, S.; Kubota, T.; Nakagawa, Y.; Tomishige, K. *ChemCatChem* **2010**, *2*, 547−555.
(26) Chia, M.; Pagan-Torres, Y. J.; Hibbitts, D.; Tan, Q.; Pham, H. N.; Datye, A. K.; Neurock, M.; Davis, R. J.; Dumesic, J. A. *J. Am. Chem. Soc.* **2011**, *133*, 12675−12689.
(27) Chen, K.; Mori, K.; Watanabe, H.; Nakagawa, Y.; Tomishige, K. *J. Catal.* **2012**, *294*, 171−183.
(28) Gilkey, M. J.; Panagiotopoulou, P.; Mironenko, A. V.; Jenness, G. R.; Vlachos, D. G.; Xu, B. *ACS Catal.* **2015**, *5*, 3988−3994.
(29) Panagiotopoulou, P.; Vlachos, D. G. *Appl. Catal., A* **2014**, *480*, 17−24.
(30) Panagiotopoulou, P.; Martin, N.; Vlachos, D. G. *J. Mol. Catal. A: Chem.* **2014**, *392*, 223−228.
(31) Balakrishnan, M.; Sacia, E. R.; Sreekumar, S.; Gunbas, G.; Gokhale, A. A.; Scown, C. D.; Toste, F. D.; Bell, A. T. *Proc. Natl. Acad. Sci. U. S. A.* **2015**, *112*, 7645−7649.
(32) Green, S. K.; Patet, R. E.; Nikbin, N.; Williams, C. L.; Chang, C.-C.; Yu, J.; Gorte, R. J.; Caratzoulas, S.; Fan, W.; Vlachos, D. G. *Appl. Catal., B* **2016**, *180*, 487−496.
(33) Chang, C.-C.; Green, S. K.; Williams, C. L.; Dauenhauer, P. J.; Fan, W. *Green Chem.* **2014**, *16*, 585−588.
(34) Abild-Pedersen, F.; Greeley, J.; Studt, F.; Rossmeisl, J.; Munter, T.; Moses, P. G.; Skulason, E.; Bligaard, T.; Nørskov, J. K. *Phys. Rev. Lett.* **2007**, *99*, 016105.
(35) Nørskov, J. K.; Bligaard, T.; Logadottir, A.; Bahn, S.; Hansen, L. B.; Bollinger, M.; Bengaard, H.; Hammer, B.; Sljivancanin, Z.; Mavrikakis, M. *J. Catal.* **2002**, *209*, 275−278.
(36) Fernández, E. M.; Moses, P. G.; Toftelund, A.; Hansen, H. A.; Martínez, J. I.; Abild-Pedersen, F.; Kleis, J.; Hinnemann, B.; Rossmeisl, J.; Bligaard, T. *Angew. Chem., Int. Ed.* **2008**, *47*, 4683−4686.
(37) Calle-Vallejo, F.; Inoglu, N. G.; Su, H.-Y.; Martínez, J. I.; Man, I. C.; Koper, M. T.; Kitchin, J. R.; Rossmeisl, J. *Chem. Sci.* **2013**, *4*, 1245−1249.
(38) Gazdzicki, P.; Jakob, P. *J. Phys. Chem. C* **2010**, *114*, 2655−2663.
(39) Shi, S.-K.; Schreifels, J.; White, J. *Surf. Sci.* **1981**, *105*, 1−19.
(40) Hammer, B.; Nørskov, J. K. *Adv. Catal.* **2000**, *45*, 71−129.
(41) Calle-Vallejo, F.; Loffreda, D.; Koper, M. T.; Sautet, P. *Nat. Chem.* **2015**, *7*, 403−410.
(42) Jae, J.; Zheng, W.; Karim, A. M.; Guo, W.; Lobo, R. F.; Vlachos, D. G. *ChemCatChem* **2014**, *6*, 848−856.
(43) Over, H.; Seitsonen, A. P.; Lundgren, E.; Schmid, M.; Varga, P. *Surf. Sci.* **2002**, *515*, 143−156.
(44) Kim, S. H.; Wintterlin, J. *J. Chem. Phys.* **2009**, *131*, 064705−064705.
(45) Guo, W.; Vlachos, D. G. *Nat. Commun.* **2015**, *6*, 8619.
(46) Green, I. X.; Tang, W.; Neurock, M.; Yates, J. T. *Science* **2011**, *333*, 736−739.
(47) Fujimoto, K.-i.; Ribeiro, F. H.; Avalos-Borja, M.; Iglesia, E. *J. Catal.* **1998**, *179*, 431−442.
(48) Guzman, J.; Carrettin, S.; Corma, A. *J. Am. Chem. Soc.* **2005**, *127*, 3286−3287.
(49) Campbell, C. T.; Peden, C. H. *Science* **2005**, *309*, 713−714.
(50) Over, H.; Kim, Y.; Seitsonen, A.; Wendt, S.; Lundgren, E.; Schmid, M.; Varga, P.; Morgante, A.; Ertl, G. *Science* **2000**, *287*, 1474−1476.
(51) Qiao, B.; Wang, A.; Yang, X.; Allard, L. F.; Jiang, Z.; Cui, Y.; Liu, J.; Li, J.; Zhang, T. *Nat. Chem.* **2011**, *3*, 634−641.
(52) Zhai, Z.; Wang, X.; Licht, R.; Bell, A. T. *J. Catal.* **2015**, *325*, 87−100.
(53) Knapp, M.; Crihan, D.; Seitsonen, A.; Resta, A.; Lundgren, E.; Andersen, J. N.; Schmid, M.; Varga, P.; Over, H. *J. Phys. Chem. B* **2006**, *110*, 14007−14010.
(54) Ferrin, P.; Kandoi, S.; Nilekar, A. U.; Mavrikakis, M. *Surf. Sci.* **2012**, *606*, 679−689.
(55) Tang, W.; Hu, Z.; Wang, M.; Stucky, G. D.; Metiu, H.; McFarland, E. W. *J. Catal.* **2010**, *273*, 125−137.
(56) Li, B.; Metiu, H. *J. Phys. Chem. C* **2011**, *115*, 18239−18246.
(57) Mayernick, A. D.; Janik, M. J. *J. Catal.* **2011**, *278*, 16−25.
(58) Sun, X.; Li, B.; Metiu, H. *J. Phys. Chem. C* **2013**, *117*, 7114−7122.
(59) Driscoll, D. J.; Lunsford, J. H. *J. Phys. Chem.* **1985**, *89*, 4415−4418.
(60) Henderson, M. A.; Epling, W. S.; Peden, C. H.; Perkins, C. L. *J. Phys. Chem. B* **2003**, *107*, 534−545.
(61) Knapp, M.; Crihan, D.; Seitsonen, A.; Lundgren, E.; Resta, A.; Andersen, J. N.; Over, H. *J. Phys. Chem. C* **2007**, *111*, 5363−5373.
(62) Yamashita, M.; Kawamura, T.; Suzuki, M.; Saito, Y. *Bull. Chem. Soc. Jpn.* **1991**, *64*, 272−278.
(63) de Barros, R. B.; Garcia, A. R.; Ilharco, L. M. *Surf. Sci.* **2002**, *502*, 156−163.
(64) Goulas, K.; Vlachos, D. G. Unpublished data.
(65) Dronskowski, R.; Bloechl, P. E. *J. Phys. Chem.* **1993**, *97*, 8617−8624.
(66) Deringer, V. L.; Tchougréeff, A. L.; Dronskowski, R. *J. Phys. Chem. A* **2011**, *115*, 5461−5466.
(67) Maintz, S.; Deringer, V. L.; Tchougréeff, A. L.; Dronskowski, R. *J. Comput. Chem.* **2013**, *34*, 2557−2567.
(68) Pang, S. H.; Román, A. M.; Medlin, J. W. *J. Phys. Chem. C* **2012**, *116*, 13654−13660.
(69) Schulz, K. H.; Cox, D. F. *J. Phys. Chem.* **1993**, *97*, 647−655.
(70) Sitthisa, S.; Sooknoi, T.; Ma, Y.; Balbuena, P. B.; Resasco, D. E. *J. Catal.* **2011**, *277*, 1−13.
(71) Deutsch, K. L.; Shanks, B. H. *J. Catal.* **2012**, *285*, 235−241.
(72) Rao, R. S.; Baker, R. T. K.; Vannice, M. A. *Catal. Lett.* **1999**, *60*, 51−57.
(73) Pang, S. H.; Schoenbaum, C. A.; Schwartz, D. K.; Medlin, J. W. *Nat. Commun.* **2013**, *4*, 2448.
(74) Wang, S.; Vorotnikov, V.; Vlachos, D. G. *ACS Catal.* **2015**, *5*, 104−112.
(75) McManus, J. R.; Vohs, J. M. *Surf. Sci.* **2014**, *630*, 16−21.
(76) Sullivan, M. M.; Chen, C.-J.; Bhan, A. *Catal. Sci. Technol.* **2016**, *6*, 602−616.
(77) Getsoian, A. B.; Shapovalov, V.; Bell, A. T. *J. Phys. Chem. C* **2013**, *117*, 7123−7137.
(78) Getsoian, A. B.; Zhai, Z.; Bell, A. T. *J. Am. Chem. Soc.* **2014**, *136*, 13684−13697.
(79) Dietl, N.; Schlangen, M.; Schwarz, H. *Angew. Chem., Int. Ed.* **2012**, *51*, 5544−5555.
(80) Wang, J.; Fan, C. Y.; Sun, Q.; Reuter, K.; Jacobi, K.; Scheffler, M.; Ertl, G. *Angew. Chem., Int. Ed.* **2003**, *42*, 2151−2154.
(81) Hoffmann, R. *Rev. Mod. Phys.* **1988**, *60*, 601.
(82) Interaction between the surface and the H_2 molecule in the transition state (TS) was calculated as a difference between the TS energy (slab+H_2), energy of the H_2 molecule at the TS geometry in a vacuum with the slab removed (singlet state), and energy of the slab at the TS geometry with H_2 removed. H_2 and slab deformation energies were calculated as energy differences between H_2 and RuO_2 slab in their TS and relaxed geometries.
(83) Kresse, G.; Hafner, J. *Phys. Rev. B: Condens. Matter Mater. Phys.* **1993**, *47*, 558.
(84) Kresse, G.; Hafner, J. *Phys. Rev. B: Condens. Matter Mater. Phys.* **1994**, *49*, 14251.
(85) Kresse, G.; Furthmüller, J. *Comput. Mater. Sci.* **1996**, *6*, 15−50.
(86) Kresse, G.; Furthmüller, J. *Phys. Rev. B: Condens. Matter Mater. Phys.* **1996**, *54*, 11169.
(87) Teschner, D.; Farra, R.; Yao, L.; Schlögl, R.; Soerijanto, H.; Schomäcker, R.; Schmidt, T.; Szentmiklósi, L.; Amrute, A. P.; Mondelli, C. *J. Catal.* **2012**, *285*, 273−284.

DOI: 10.1021/jacs.6b02871
J. Am. Chem. Soc. 2016, 138, 8104−8113

(88) Over, H. *Chem. Rev. (Washington, DC, U. S.)* **2012**, *112*, 3356−3426.
(89) Perdew, J. P.; Burke, K.; Ernzerhof, M. *Phys. Rev. Lett.* **1996**, *77*, 3865.
(90) De Almeida, J.; Ahuja, R. *Phys. Rev. B: Condens. Matter Mater. Phys.* **2006**, *73*, 165102.
(91) Reuter, K.; Frenkel, D.; Scheffler, M. *arXiv preprint cond-mat/0408080* 2004.
(92) Grimme, S.; Antony, J.; Ehrlich, S.; Krieg, H. *J. Chem. Phys.* **2010**, *132*, 154104.
(93) Kee, R.; Rupley, F.; Miller, J. *Chemkin-Ii: A Fortran Chemical Kinetics Package for the Analysis of Gas-Phase Chemical Kinetics*; Sandia National Laboratories: Albuquerque, NM, 1989.
(94) Coltrin, M. E.; Kee, R. J.; Rupley, F. *Surface Chemkin (Version 4.0): A Fortran Package for Analyzing Heterogeneous Chemical Kinetics at a Solid-Surface---Gas-Phase Interface*; Sandia National Labs., Livermore, CA (United States), 1991.

DOI: 10.1021/jacs.6b02871
J. Am. Chem. Soc. 2016, 138, 8104−8113